

Faster GPU-based convolutional gridding via thread coarsening

Bruce Merry^a

^aSKA South Africa, 3rd Floor, The Park, Park Road, 7405 South Africa

Abstract

Convolutional gridding is a processor-intensive step in interferometric imaging. While it is possible to use graphics processing units (GPUs) to accelerate this operation, existing methods use only a fraction of the available flops. We apply thread coarsening to improve the efficiency of an existing algorithm, and observe performance gains of up to 3.2× for single-polarization gridding and 1.9× for quad-polarization gridding on a GeForce GTX 980, and smaller but still significant gains on a Radeon R9 290X.

Keywords: techniques: interferometric, methods: numerical, computing methodologies: graphics processors

1. Introduction

Interferometric imaging is a key tool in radio astronomy, but as modern instruments provide more antennas, longer baselines, and more channels, it is becoming increasingly computationally costly. A major component of an imaging pipeline is *convolutional gridding*, as well as the corresponding degridting for predicting visibilities.

Given the computational cost of gridding, it is natural to apply accelerator hardware, of which the cheapest and most ubiquitous is the Graphics Processing Unit (GPU). However, the irregular data access patterns make this a non-trivial task. One of the first really practical algorithms for GPU-accelerated gridding is due to Romein (2012). Despite being state of the art, it typically spends only about 25% of a GPU's compute power on the actual convolution operations. There are bottlenecks in the memory system, but also computational overheads associated with address calculations. Our goal is to reduce these overheads to make more flops available for the convolution calculations.

Our contribution is a modification to the algorithm in which each thread of execution processes multiple elements of the grid. This is a standard transformation called *thread coarsening*, but which we have adapted to this specific problem. This allows some overheads to be amortized across multiple grid elements, thus increasing performance.

2. Background

2.1. Graphics Processing Units

While originally designed for computer graphics, GPUs have become a common and accessible approach to accelerating general-purpose computations. Here we provide

only a brief introduction to GPU architecture; a complete discussion is beyond the scope of this paper. Two common APIs used to program GPUs are CUDA (a proprietary standard from NVIDIA), and OpenCL (a cross-vendor standard that is also applicable to CPUs and FPGAs). We will use the OpenCL terminology as it is more generic, although our implementation runs on both CUDA and OpenCL. For readers more familiar with CUDA, substitute thread for work-item, thread-block for work-group, grid for kernel-instance, shared memory for local memory, and streaming multiprocessor for compute unit.

OpenCL works on a single-program multiple-data model. A single program, called a *kernel*, is executed many times in parallel. Each execution is a *work-item*. Work-items are arranged into *work-groups*. The work-items of a work-group are guaranteed to execute concurrently, and can synchronize and communicate with each other. The set of all work-items launched at one time is called a *kernel-instance*. GPUs comprise multiple *compute units* which operate largely independently, each with their own schedulers, L1 caches, register file and execution units — similar to CPU cores. Each work-group is assigned to one compute unit, but a compute unit can run multiple work-groups concurrently.

GPUs also have multiple memory systems. The slowest, largest memory is *global memory*, which is generally off-chip DRAM. There are usually also several levels of cache for this global memory. *Local memory* is fast on-chip memory local to a compute unit, which can be used for work-items in a work-group to communicate with each other, and is also used as a software-managed cache. The fastest memory is registers, which are local to a work-item. There are other special-purpose memory types, but they are not relevant here.

Email address: bmerry@ska.ac.za (Bruce Merry)

2.2. Convolutional Gridding

Consider the full-Sky radio interferometry measurement equation (RIME) (Smirnov, 2011, eq 17):

$$K_{pq} = e^{-2\pi i(u_{pq}l + v_{pq}m + w_{pq}(n-1))}$$

$$V_{pq} = G_p \left(\iint_{lmn} \frac{1}{n} K_{pq} E_p B E_q^H dl dm \right) G_q^H. \quad (1)$$

Here, l, m, n are direction cosines parameterizing the sky, (u_{pq}, v_{pq}, w_{pq}) is the baseline vector between antennas p and q , B is the brightness matrix at (l, m, n) , E_p is a Jones matrix for direction-dependent effects, G_p is a Jones matrix for direction-independent effects, and V_{pq} is the predicted visibility.

With the exception of the $w_{pq}(n-1)$ term in the exponent, this is a Fourier transform relationship between visibilities and the sky. Evaluating or inverting the RIME directly is prohibitively expensive, so it is typically done using fast Fourier transforms (FFTs) (Cooley and Tukey, 1965). However, visibilities are not sampled on a regular grid, so an extra *gridding* step must be taken to generate such a grid before using the FFT to produce an image.

Simply snapping each visibility sample to the nearest point on the grid would cause severe artefacts, particularly aliasing. Instead, each visibility sample is treated as a Dirac delta, convolved with some function, and then sampled onto the grid. Convolution in visibility space is equivalent to multiplication in image space, so using a function with bounded support in image space provides antialiasing (Greisen, 1979). The $e^{w_{pq}(n-1)}$ and E_p terms can also be handled by convolution in visibility space — these are known as W-projection (Cornwell et al., 2008) and A-projection (Bhatnagar et al., 2006) respectively.

The gridding convolution function (GCF) cannot always be computed analytically, and even when it can, it is usually expensive to do so. Thus, tables of GCFs are normally precomputed numerically. To reduce aliasing, the GCF needs to be sampled at a higher resolution than the grid itself. A typical value is $8\times$ oversampling (Romein, 2012), but this will depend on how far from the field of view one expects to find contaminating signals.

Efficient gridding on a GPU is challenging because the problem has irregular structure, with the memory accesses depending on the uvw coordinates. There is plenty of parallelism, but multiple visibilities will contribute to each grid point and so there are data hazards. A naïve implementation will also be totally memory-bound: multiplying two single-precision complex numbers and accumulating the result into memory requires 8 flops and 16 bytes of memory traffic, while typical desktop GPUs can have compute-to-bandwidth ratios of 15–20 flops per byte.

Romein (2012) introduced the first reasonably efficient GPU-accelerated gridding algorithm. It takes advantage of the spatial coherence of the data to reduce memory bandwidth. For a single baseline and frequency, the UV-plane positions move slowly over time as the Earth rotates. Similarly, moving to an adjacent frequency bin involves a

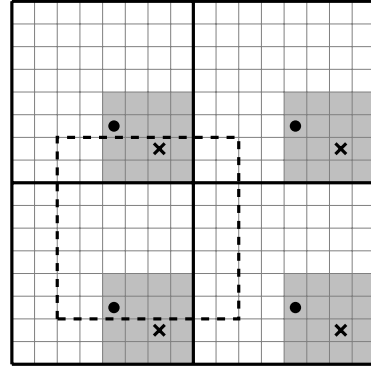


Figure 1: Overview of Romein’s gridding algorithm. The dashed box shows a bounding box containing the GCF footprint. One work-item handles grid points marked with a dot; another handles those marked with a cross, and so on. The gray box indicates a tile: once all the grid points in a tile have been handled, the same work-items are recycled to update the next tile.

small shift in the UV plane. Thus, if one iterates over the visibilities for a single baseline, the GCF footprints will almost entirely overlap. This makes it possible to maintain sums in registers which are only occasionally flushed to global memory.

Figure 1 shows how the algorithm works. The grid is divided into *bins*, which are at least as large as the GCF — in the original algorithm, they are the same size. A work-item is responsible for all the positions in the grid that have the same relative placement within a bin, e.g., all the grid positions marked with a dot are the responsibility of one work-item. A bin-sized bounding box is placed around the GCF footprint for one visibility, which will contain exactly one grid-point per work-item. Each work-item maintains an in-register accumulator for that grid point. When the bounding box moves, some work-items will switch to a different grid point: when this happens, those work-items flush their accumulator to global memory using an atomic addition. If the bounding box moves by one grid point, then only $O(N)$ atomic updates are made for an $N \times N$ GCF, thus greatly reducing the memory traffic.

Coarse-grained parallelism is achieved by assigning each baseline to a separate work-group. Because these work-groups operate independently, they may potentially update the same grid points at the same time; this is why grid updates are done using atomic instructions.

A complication arises if the bins are too large to hold an entire bin in registers at once. In this case, each bin is split into *tiles* (Figure 1 shows one tile in gray), and a work-group handles only one tile’s-worth of work-items. Romein iterates serially over tiles within the GPU code: after a work-group has iterated over all visibilities in its baseline, it iterates over them again, but taking responsibility for the next tile. Our implementation is parallel rather than serial, using a separate work-group per tile. In either case, the number of atomic updates to the grid is unaffected by tile size, but visibilities and their coordinates are loaded from memory once for each tile in a bin.

Muscat (2014) noticed that it is not necessary to grid each visibility individually. In some cases, particularly for short baselines, two adjacent visibilities have the same position on the higher-resolution grid used to sample the GCF. This means that they will be multiplied by the same GCF samples, and thus they can be added together to form a single visibility. This yields identical results (up to floating-point precision) but reduces the number of visibilities to grid. He refers to this merging process as *compression*. We use compression in our implementation, and in our results we consider only the rate for gridding these compressed visibilities, rather than the original visibilities.

3. Thread Coarsening

Thread coarsening is the process of merging multiple work-items (also known as threads) into one. This is similar to loop unrolling, but applied across parallel work-items rather than across serial loop iterations. This improves instruction-level parallelism (Volkov and Demmel, 2008), reduces the number of memory-access instructions (Yang et al., 2012) and eliminates redundant calculations when the same value is computed in every work-item (Magni et al., 2013).

Thread coarsening also has several negative effects. It reduces the total amount of parallelism, which can harm performance if there is insufficient remaining parallelism to saturate the GPU. It increases the number of registers used per work-item, which in turn reduces the number of work-items that can execute in parallel (*occupancy*). All else being equal, reducing occupancy will reduce latency-hiding, but with thread-coarsening it is compensated by the increase in instruction-level parallelism (Volkov, 2010). Finally, it can modify memory access patterns such that an access by a sub-group is no longer to contiguous memory (so-called *coalesced* access), thus requiring more transactions with the memory system.

Thread-coarsening can be automated by a compiler, but for gridding this will not achieve the full benefits. The address calculations in Romein’s algorithm are different for each work-item, so thread-coarsening would not reduce the number of instructions required. However, adjacent work-items mostly access adjacent memory locations — the exception being when they are at the edge of the bounding box, causing wrap-around. We can eliminate this case by having the bounding box move in larger steps, so that it is always aligned to a coarser grid. This allows most of the work in address calculation to be amortized across multiple grid points.

Figure 2 shows how this is implemented. Each work-item now handles a *block* of grid points (2×2 in the figure), and the bounding box is aligned to the edges of blocks. Of course, the footprint of the GCF is unaffected, so the bounding box must now be slightly larger than the GCF to ensure that a suitably aligned bounding box can always be found to contain the GCF. Grid-point updates still occur for the grid points in the padding between the GCF

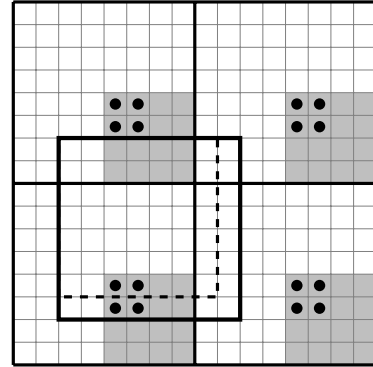


Figure 2: Mapping of work-items and work-groups to grid points. One work-group contributes to all the shaded cells. One work-item contributes to all the cells marked with a dot. Here blocks are 2×2 , tiles are 4×4 and bins are 8×8 . The dashed box shows a GCF footprint, and the solid box shows the bounding rectangle.

footprint and the bounding box, so the storage for the GCF must be padded with zeros. These updates are also wasted computations, but provided the blocks are significantly smaller than the GCF, this will add only a small amount of overhead.

With this change, expensive address calculations that were previously done per grid point are now only done once per block. In particular, it is only necessary to check whether the whole block has moved out of the bounding box, rather than each grid point. This reduces the total number of instructions needed for addressing and thus frees up more cycles for actual gridding calculations.

4. Implementation Details

Muscat (2014) implements compression on the fly during gridding. For deconvolution with major cycles (Schwab, 1984), the compression only needs to be done once for all cycles, so we have implemented it as a preprocess. For each compressed visibility, the gridding kernel receives the integer grid coordinates, the sub-grid coordinates for indexing the GCF, the w plane index, and the pre-weighted visibility values. Rather than all work-items directly loading these values from global memory, they are staged via local memory in batches. When loading a batch, each work-item loads one visibility.

We found that the NVIDIA CUDA compiler was causing the kernels to use far more registers than we expected. Examining the assembly code, we found that it was using extra scratch registers for flushing accumulators. The CUDA C code would first atomically add the accumulator to global memory, then set it to zero. The assembly code instead copied the accumulator to a temporary, zeroed the accumulator, then atomically added the temporary to global memory. This was presumably done to improve latency-hiding (allowing the accumulator to be re-used before the atomic operation completed). However, this increases the number of 32-bit registers by two times

the number of polarizations times the coarsening factor. In this case, the extra register pressure reduced occupancy so much that performance dropped overall. As a workaround, we added the statement `asm("")` as a compiler-level memory barrier.

Romein (2012) found that the majority of memory traffic was due to cache misses in reading the convolution GCF values. To avoid this problem, we have used a separable approximation to the GCF (Merry, 2016). We have also (like Romein) assumed that the GCF is polarization-independent. Both these assumptions mean that our results cannot be directly applied to A-projection; we nevertheless expect our technique to provide similar accelerations for A-projection, provided the memory system can keep up.

Coarsening also works nicely with a separable GCF. For an $m \times n$ block, we load $m + n$ values from memory in each work-item, and compute the $m \times n$ products in registers. Larger blocks thus reduce the number of memory transactions required.

It is difficult to determine the best coarsening factors and work-group size theoretically, because there are trade-offs. For example, a larger work-group implies fewer tiles per bin, and thus less memory traffic to load visibilities; but only an integer number of work-groups can be active on a compute unit at a time, so larger work-groups may cause resources to be under-utilised. We have dealt with this by using autotuning: a small artificial data-set is synthesized and benchmarked with a range of coarsening factors and work-group sizes, and the best combination is remembered. We perform auto-tuning separately for each number of polarizations.

Another tuning factor is the number of visibilities to process in each work-group. Romein (2012) uses one work-group per baseline; but with compression, that will lead to unbalanced workloads. We order visibilities by baseline, but assign a fixed number of visibilities to each work-group. Larger numbers make more use of spatial coherence between adjacent visibilities, but reduce parallelism. Our current implementation uses 1024 per work-group.

5. Results

We found that the performance of our gridding implementation is highly dependent on the coordinates and ordering of the data. To obtain a dataset that is representative of future radio telescopes, we simulate a single-channel, two-hour observation on MeerKAT (SKA South Africa, 2015) with a 2 s integration time, and compressed the visibilities. These compressed visibilities are available online ¹ for anyone who wishes to do a direct comparison. All gridding calculations are done in single-precision floating point.

¹<https://github.com/ska-sa/thread-coarsening-grid-data>

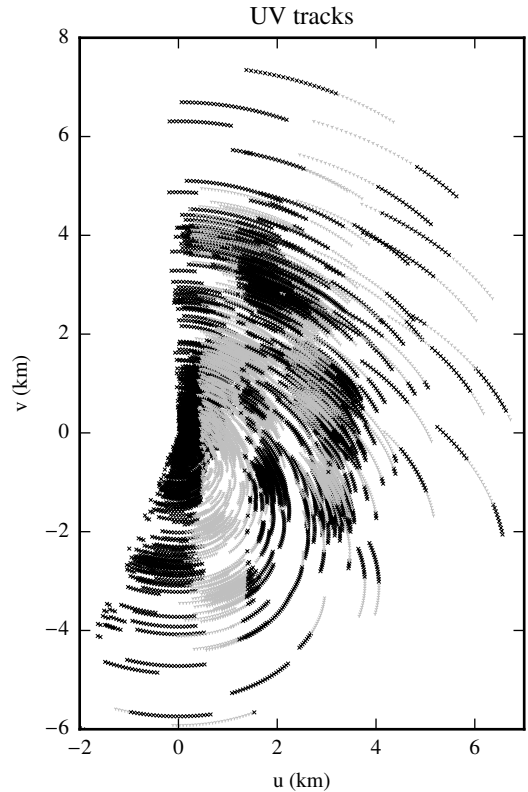


Figure 3: The uv coordinates in our simulation. To improve legibility, only every 100th visibility is shown. The alternating bands of black and gray correspond to the slices used for W-stacking (they overlap because the array is not perfectly coplanar).

Pure W-projection requires large GCFs to correct the W effects, making it very slow. For MeerKAT, we expect it to be used in conjunction with techniques such as W-stacking (Offringa et al., 2014). We have thus split the data into a number of slices by w value, as shown in Figure 3. We invoke a separate kernel-instance for each slice in the stack. There are 7 slices with a total of 2 337 867 compressed visibilities (from 7 257 600 uncompressed), and 1229 W planes per slice. Note that in real use, the number of slices would be adapted to the size of the GCF (or vice versa), but we have kept the number of slices fixed while varying the GCF size so that we can study the effect of GCF size in isolation.

It should be emphasized that these choices are largely conservative. The use of such a short observation with a single channel, which is further split into W slices, substantially reduces parallelism. The results reported here are thus likely to be achievable in other configurations.

We explored a variety of configurations: coarsening factor of 1, 2, 4 or 8 on each axis (up to a combined factor of 16), work-group size of 4, 8 or 16 on each axis, bin sizes of 32, 64 or 128; and either 1 or 4 polarizations. The GCF size was computed as $\text{bin size} + 1 - \max(\text{coarsen}_u, \text{coarsen}_v)$, which is the largest square size possible.

We report results on two GPUs: an NVIDIA GTX 980 (Maxwell architecture) using CUDA, and an AMD Radeon

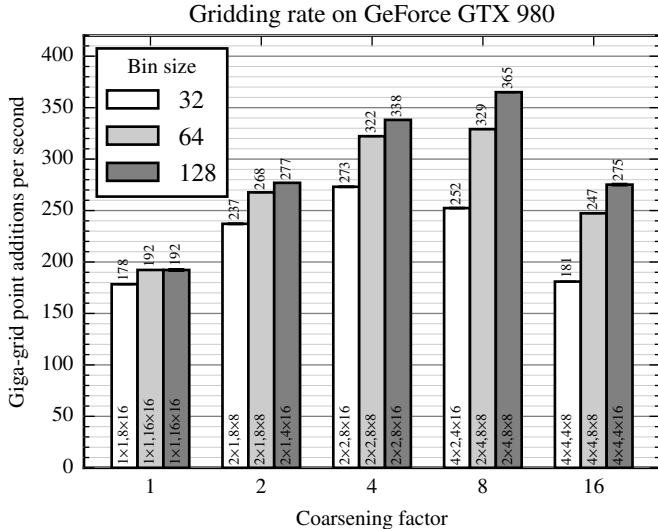


Figure 4: Gridding rates for four polarizations (GTX 980). The numbers inside the bars are the coarsening factors (in U and V), and the number of work-items per work-group (in U and V) in the best case.

R9 290X (GCN architecture) using OpenCL. These have theoretical single-precision performance of 5.288 Tflop/s and 5.632 Tflop/s, and memory bandwidth of 224 GB/s and 352 GB/s respectively. The implementation was developed and tuned on the Maxwell architecture, so we give the most attention to results on the GTX 980, and results are for this GPU except where otherwise noted. The R9 290X is included to show that the optimizations are not specific to one GPU architecture or API.

Figure 4 shows gridding rates for four polarizations. For each total coarsening factor, we show only the result for the best combination of U and V coarsening factors and work-group size. We consider a grid-point addition to be an addition for a single polarization, which requires 8 flops. The efficiency without coarsening is 27–29%, which is similar to (but slightly higher than) the 24% reported by Romein (2012), and much higher than the results of Muscat (2014).

In the best case (bin size 128, coarsening factor 8) we achieve 365 GGPA/s, at 55% efficiency. This is a 90% improvement over no coarsening at the same bin size. For a bin size of 32, the improvement due to coarsening is only 53%. Improvements will be less at smaller bin sizes because too much coarsening will quickly increase the proportion of flops wasted by padding and reduce the available parallelism. This can be seen in the performance drop from 4× to 8× coarsening.

Figure 5 shows gridding rates for a single polarization. Here, the ratio of address calculations to gridding calculations is four times larger, and thread coarsening makes a larger impact. For 128-pixel bins, the performance improves by a factor of 3.2. We also tested with larger coarsening factors, but they performed worse than those shown.

Figure 6 shows the utilization of the single-precision

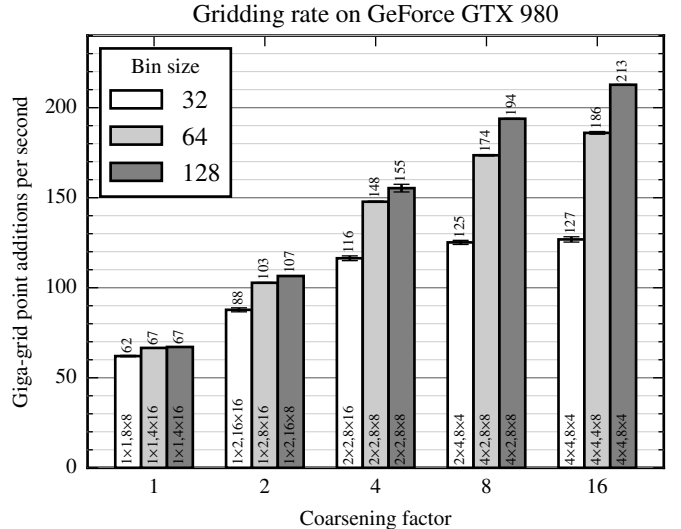


Figure 5: Gridding rates for a single polarization (GTX 980).

Table 1: Memory bandwidths for the best case (four polarizations, 128-pixel bins, 8× coarsening), on GTX 980.

Memory Type	Read (GB/s)	Write (GB/s)
Shared	292.4	9.1
Unified cache	1,255.4	0.0
L2 cache	117.2	40.1
Device	14.5	6.4

units in the GPU, which handle both floating-point and integer instructions. This shows that although utilization is not much higher for four polarizations than for one, the proportion of instructions used for convolution is much higher. The lower utilization for smaller bin sizes is largely due to a lack of parallelism in the more sparsely populated W slices — in the worst case, there are not enough work-groups to give every compute unit work to do. If we consider only the first slice, then utilization levels are all between 75% and 85%, and the NVIDIA profiler considers this to be compute-bound.

The profiler also reports bandwidths and utilization for the various memory systems. Table 1 shows the bandwidths for the best case. The decline in bandwidth from the unified cache (L1) to L2 to device (global) memory shows that the caches are effective.

We now report results for the Radeon R9 290X. Since OpenCL doesn’t support atomic additions, we had to emulate them using slower compare-and-swap operations. Since these operations are not affected by our optimizations, we expect thread coarsening to have less impact.

Figures 7 and 8 show the speedups obtained with thread coarsening on this GPU. One noticeable difference from the GTX 980 figures is that the optimal coarsening factor is lower. This suggests that register pressure is an issue, but we have not investigated whether this is due to compiler quirks such as the one we worked around for

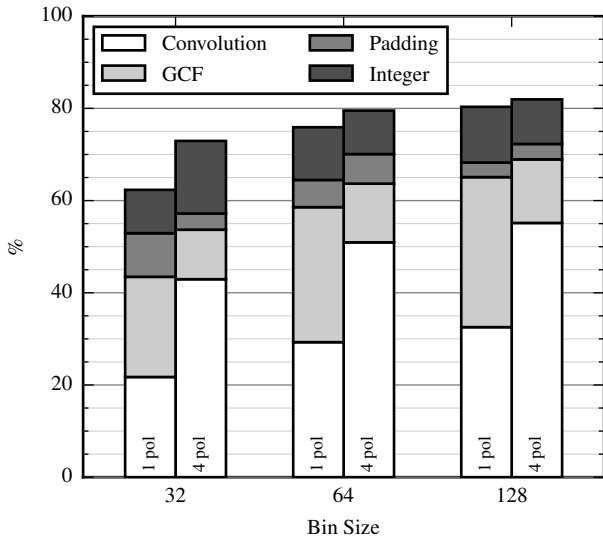


Figure 6: Utilization of the single-precision units. *Convolution*: instructions that multiply GCF samples with visibilities and accumulate the result. *GCF*: instructions to reconstruct GCF samples from the separable parts. *Padding*: flops that are wasted due to padding of the GCF.

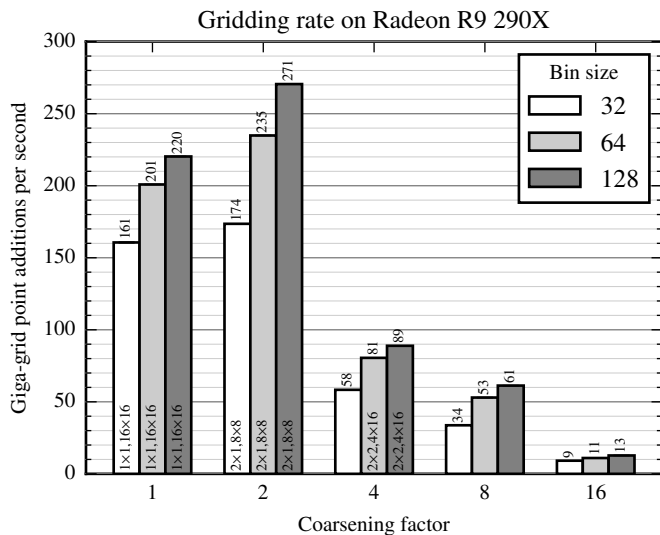


Figure 7: Gridding rates for four polarizations (R9 290X).

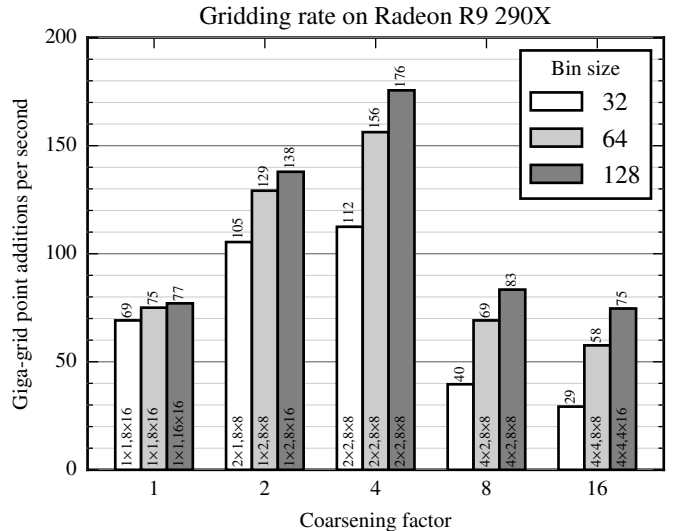


Figure 8: Gridding rates for a single polarization (R9 290X).

the NVIDIA compiler. Between the emulated atomic additions and this inability to utilize higher coarsening factors, it is not surprising that coarsening is less effective than on the GTX 980. Nevertheless, it is beneficial, with up to 23% improvement for four polarizations and 128% improvement for one polarization.

6. Conclusions and Future Work

Thread coarsening clearly provides a significant performance improvement, and we recommend that gridders based on Romein’s algorithm should use thread coarsening to improve performance, unless they use only very small GCFs (for example, because W effects are corrected by other means than W projection).

We have shown significant gains in all the tested configurations, but the largest gains are for large GCFs. The results for small GCFs are hurt by a lack of parallelism in the sparse W slices, which could be improved by adapting tuning parameters (both the coarsening factor and the number of visibilities per work-group) to the number of visibilities.

For large GCFs, performance is limited by the single-precision units, so further significant optimizations can only come from reducing the number of flops. For each visibility V , polarization p and position i, j in the GCF footprint, we need to compute the product $G_{ij}^u V_p = (G_i^u G_j^y) V_p$. We currently compute this as written, but Merry (2016) notes that fewer flops are required to compute this as $G_i^u (G_j^y V_p)$ because the factor in parentheses is independent of i . For a bin size B and number of polarizations P , this reduces the number of required multiplications from $B^2 + B^2 P$ to $BP + B^2 P$. This is not an entirely free optimization, because the common factor needs to be broadcast to all work-items that need it, but we expect that performance should still improve.

Autotuning is clearly important to find the optimum coarsening factor. Our results show that tuning needs to consider both the number of polarizations and the bin size. On the other hand, one need only consider coarsening shapes that are as square as possible i.e., in 1 : 1 or 2 : 1 ratio. This is expected, because squarer shapes reduce both the amount of zero padding and the number of memory accesses to load the separable GCF components.

Our implementation uses power-of-two sizes for bins, because this simplifies some of the integer arithmetic in coordinate calculations. However, this is not a fundamental limitation, and it would be possible to use non-power-of-two sizes at all levels of the hierarchy. This may yield further small performance improvements by providing a finer-grained set of options.

A natural next step is to apply thread coarsening to degridging in a similar fashion. Our preliminary results show that performance improvements are even better than for gridding, but we have not yet fully optimized our degridder and this may affect the results. Nevertheless, we expect thread coarsening to be important in degridging.

We have not considered A-projection in our performance measurements. A-projection requires significantly more instructions and bandwidth for loading the GCFs, because they are dependent on time, frequency, polarization and possibly baseline, and are not separable. We thus expect thread-coarsening to have a smaller effect, because bandwidth and latency considerations will play a larger part.

References

- Bhatnagar, S., Golap, K., Cornwell, T., 2006. Correction of errors due to antenna power patterns during imaging. EVLA memo 100.
- Cooley, J.W., Tukey, J.W., 1965. An algorithm for the machine calculation of complex fourier series. *Mathematics of Computation* 19, 297–301. URL: <http://www.jstor.org/stable/2003354>.
- Cornwell, T., Golap, K., Bhatnagar, S., 2008. The noncoplanar baselines effect in radio interferometry: The W-projection algorithm. *IEEE J. of Selected Topics in Signal Processing* 2, 647–657. doi:10.1109/JSTSP.2008.2005290.
- Greisen, E.G., 1979. The effects of various convolving functions on aliasing and relative signal-to-noise ratios. URL: http://library.nrao.edu/public/memos/vla/sci/VLAS_131.pdf. VLA Scientific Memorandum #131.
- Magni, A., Dubach, C., O’Boyle, M.F.P., 2013. A large-scale cross-architecture evaluation of thread-coarsening, in: *Proceedings of the International Conference on High Performance Computing, Networking, Storage and Analysis*, ACM, New York, NY, USA. pp. 11:1–11:11. URL: <http://doi.acm.org/10.1145/2503210.2503268>, doi:10.1145/2503210.2503268.
- Merry, B., 2016. Approximating W projection as a separable kernel. *MNRAS* 456, 1761–1766. URL: <http://mnras.oxfordjournals.org/content/456/2/1761.abstract>, doi:10.1093/mnras/stv2761, arXiv:<http://mnras.oxfordjournals.org/content/456/2/1761.full.pdf+html>.
- Muscat, D., 2014. High-Performance Image Synthesis for Radio Interferometry. Master’s thesis. University of Malta.
- Offringa, A.R., McKinley, B., Hurley-Walker, N., Briggs, F.H., Wayth, R.B., Kaplan, D.L., Bell, M.E., Feng, L., Neben, A.R., Hughes, J.D., Rhee, J., Murphy, T., Bhat, N.D.R., Bernardi, G., Bowman, J.D., Cappallo, R.J., Corey, B.E., Deshpande, A.A., Emrich, D., Ewall-Wice, A., Gaensler, B.M., Goeke, R., Greenhill, L.J., Hazelton, B.J., Hindson, L., Johnston-Hollitt, M., Jacobs, D.C., Kasper, J.C., Kratzenberg, E., Lenc, E., Lonsdale, C.J., Lynch, M.J., McWhirter, S.R., Mitchell, D.A., Morales, M.F., Morgan, E., Kudryavtseva, N., Oberoi, D., Ord, S.M., Pindor, B., Procopio, P., Prabu, T., Riding, J., Roshi, D.A., Shankar, N.U., Srivani, K.S., Subrahmanyan, R., Tingay, S.J., Waterson, M., Webster, R.L., Whitney, A.R., Williams, A., Williams, C.L., 2014. WSCLEAN: an implementation of a fast, generic wide-field imager for radio astronomy. *MNRAS* 444, 606–619. URL: <http://mnras.oxfordjournals.org/content/444/1/606.abstract>, doi:10.1093/mnras/stu1368, arXiv:<http://mnras.oxfordjournals.org/content/444/1/606.full.pdf+html>.
- Romein, J.W., 2012. An efficient work-distribution strategy for gridding radio-telescope data on GPUs, in: *Proc. 26th ACM Int. Conf. on Supercomputing*, ACM, New York, NY, USA. pp. 321–330. URL: <http://doi.acm.org/10.1145/2304576.2304620>, doi:10.1145/2304576.2304620.
- Schwab, F.R., 1984. Relaxing the isoplanatism assumption in self-calibration; applications to low-frequency radio interferometry. *Astron. J.* 89, 1076–1081. doi:10.1086/113605.
- SKA South Africa, 2015. MeerKAT array releases and specifications. URL: <http://public.ska.ac.za/meerkat/schedule>.
- Smirnov, O., 2011. Revisiting the radio interferometer measurement equation. I. a full-sky Jones formalism. *A&A* 527, A106. doi:10.1051/0004-6361/201016082, arXiv:1101.1764.
- Volkov, V., 2010. Better performance at lower occupancy, in: *Proceedings of the GPU Technology Conference*.
- Volkov, V., Demmel, J., 2008. Benchmarking GPUs to tune dense linear algebra, in: *International Conference for High Performance Computing, Networking, Storage and Analysis*, 2008, pp. 1–11. doi:10.1109/SC.2008.5214359.
- Yang, Y., Xiang, P., Kong, J., Mantor, M., Zhou, H., 2012. A unified optimizing compiler framework for different GPGPU architectures. *ACM Trans. Archit. Code Optim.* 9, 9:1–9:33. URL: <http://doi.acm.org/10.1145/2207222.2207225>, doi:10.1145/2207222.2207225.